BIOCHEMISTRY
including biophysical chemistry & molecular biology

ARTICLE

pubs.acs.org/biochemistry

Molecular Dynamics Simulations Reveal Insights into Key Structural Elements of Adenosine Receptors

David Rodríguez,[†] Ángel Piñeiro,[‡] and Hugo Gutiérrez-de-Terán*[,†]

[†]Fundación Pública Galega de Medicina Xenómica, Hospital Clínico Universitario de Santiago (CHUS), planta-2, A Choupana, s/n E-15706 Santiago de Compostela, Spain

[‡]Soft Matter and Molecular Biophysics Group, Department of Applied Physics, University of Santiago de Compostela, Campus Vida s/n, E-15782 Santiago de Compostela, Spain

Supporting Information

ABSTRACT: The crystal structure of the human A_{2A} adenosine receptor, a member of the G protein-coupled receptor (GPCR) family, is used as a starting point for the structural characterization of the conformational equilibrium around the inactive conformation of the human A_2 (A_{2A} and A_{2B}) adenosine receptors (ARs). A homology model of the closely related A_{2B}AR is reported, and the two receptors were simulated in their apo form through all-atom molecular dynamics (MD) simulations. Different conditions were additionally explored in the A_{2A}AR, including the protonation state of crucial histidines or the presence of the cocrystallized ligand. Our simulations reveal the role of several conserved residues in the ARs in the conformational equilibrium of the receptors. The "ionic lock" absent in the crystal structure of the inactive A_{2A}AR is rapidly formed in the two simulated receptors, and a complex network of interacting residues is presented that further stabilizes this structural element. Notably, the observed rotameric transition of Trp6.48 ("toggle switch"), which is thought to initiate the activation process in GPCRs, is accompanied by a concerted rotation of the conserved residue of the A_2ARs, His6.52. This new conformation is further stabilized in the two receptors under study by a novel interaction network involving residues in transmembrane (TM) helices TM5 (Asn5.42) and TM3 (Gln3.37), which resemble the conformational changes recently observed in the agonist-bound structure of β-adrenoreceptors. Finally, the interaction between Glu1.39 and His7.43, a pair of conserved residues in the family of ARs, is found to be weaker than previously thought, and the role of this interaction in the structure and dynamics of the receptor is thoroughly examined. All these findings suggest that, despite the commonalities with other GPCRs, the conformational equilibrium of ARs is also modulated by specific residues of the family.

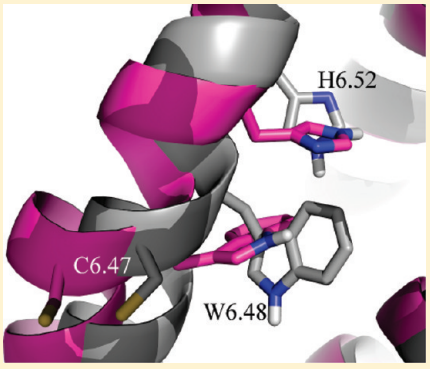

G protein-coupled receptors (GPCRs), the largest family of membrane receptors in the human genome, are transmembranal proteins in charge of the transduction of signals across cellular membranes.[1] A delicate conformational equilibrium between extreme active and inactive forms of these receptors is behind the signal transduction, which is modulated toward activation by the binding of their respective natural agonist.[2] From a structural point of view, GPCRs share a conserved topology: a helical bundle consisting of seven transmembrane (TM) helices spanning the membrane, which are connected by three extracellular (EL) and three intracellular (IL) loops. Recent advances in structural biology have revealed that the largest differences among GPCRs are located in their extracellular halves, where ligand binding occurs.[3] A general phylogenetic classification of the GPCR superfamily[4] shows well-defined clusters, which can be related to the chemical nature of the receptor's natural ligand.

Adenosine receptors (ARs) make up one family of GPCRs, which mediate the important extracellular role of the nucleoside adenosine. Four AR subtypes exist, namely, A_1, A_{2A}, A_{2B}, and A_3, with different signaling functions and tissue distributions. The pharmacological interest in ARs as drug targets is widely recognized because of the variety and importance of the physiological functions mediated by them, as well as the associated pathologies.[5] Pharmacological applications of AR chemical modulators include several inflammatory processes, where the role of the A_{2A}AR and A_3AR is generally accepted,[6] or several respiratory pathological events such as allergic asthma, where the nonselective AR antagonist theophylline is one of the main treatments, although more selective A_{2B}AR antagonists are in clinical trials.[7] The use of adenosine itself in the treatment of certain arrhythmias and the anti-infarct effect of other adenosine agonists is mediated by the A_1AR,[8] while the A_{2A}AR is involved in vascular diseases such as hypertension or atherosclerosis.[9] ARs are also involved in neural regulation in the central nervous system, as exemplified by the well-known AR antagonist caffeine.[10]

Received: January 21, 2011
Revised: April 11, 2011
Published: April 11, 2011

The recent discovery of A_{2A}AR−dopamine D_2 receptor heterodimers in ganglial neurons led to increased interest in the A_{2A}AR as a target for Alzheimer's disease.[11]

Given the high degree of biomedical relevance of the AR family members, it is not difficult to understand the breakthrough that meant the release of the hA_{2A}AR crystal structure at a resolution of 2.6 Å.[12] The structure represents one of the inactive states of the receptor with the subtype selective high-affinity antagonist ZM241385 bound to it. As in the case of the human β2-adrenergic receptor (hβ2),[13] stabilization of the receptor was achieved by substitution of the third intracellular loop (IL3) with the T4 bacteriophage lysozyme (T4L fusion protein strategy). The long C-terminus (Ala^{317}−Ser^{412}) was deleted, while the first two residues of the N-terminus and seven residues (149−155) of the second extracelluar loop (EL2) were not determined,[14] which probably indicated the high mobility of these regions. Despite these limitations, the structure of the A_{2A}AR—ZM241385 complex has revealed important particular features of the AR family and offers a new scenario for the study of the ARs, considering the high degree of sequence identity within their members. As recently reviewed, the helical bundle orientation and packing is similar among the GPCRs with known structures.[3] The major differences are located in the loop regions and within the binding site cavity. It is precisely the A_{2A}AR that shows the most divergence: the conformations of EL2 and EL3 are constrained because of the presence of three extra disulfide bonds, besides the one conserved in all GPCRs between EL2 and TM3. Additionally, the binding site not only is more shifted toward helices TM6 and TM7, as previously suggested by site-directed mutagenesis and molecular modeling studies of ARs,[15] but also includes important direct interactions of residues at EL2 with the cocrystallized ligand.

Until very recently, GPCR crystal structures had been determined with either an antagonist or an inverse agonist bound, thus stabilizing an inactive conformation of the receptor. An exception to this rule was the opsin, the ligand-free active form of rhodopsin,[16] followed by very recent structures of β-adrenergic receptors in different activelike conformations.[17−19] The elucidation of the structure and dynamic pathways, connecting the ensemble of conformational states of a GPCR,[2] is a question of major interest. According to the currently accepted GPCR activation theories, two structural elements play a key role in the activation process: (i) a salt bridge formed by residue Arg3.50 (see Materials and Methods for residue numbering), belonging to the (E/D)RY motif, and Glu6.30 known as an "ionic lock"[20,21] and (ii) the "toggle switch", a term that refers to the rotameric transition of Trp6.48 in TM6.[22] While some authors propose that a connection should exist between these two events,[23] biophysical experiments with the β2-adrenergic receptor suggest that the disruption of the ionic lock and the activation of the rotameric toggle switch are not tightly coupled.[24] The ionic lock is present in the inactive crystal structure of bovine rhodopsin but not in the experimental structure representing a model of the active form (opsin),[16] which has led to the idea that the rupture of this salt bridge is a switch in the activation process. Whereas the very recently determined structure of the inactive D_3 dopamine receptor (D_3DR) shows a formed ionic lock,[25] a disrupted TM3−TM6 ionic lock is observed in the rest of the GPCRs crystallized in the inactive form (hA_{2A}AR and tβ1- and hβ2-adrenergic receptors).[1] A comparison of active and inactive forms of (rhod)opsins reveals that the degree of TM6 bending is lower in the active conformation. This is accompanied by an extension of the TM5 and TM6 helical segments in their intracellular part. Such observations are in agreement with the activation theories proposed for the family of adrenergic receptors[22] and further confirmed by the very recently determined crystal structure of the nanobody-stabilized active state of hβ2.[19] Interestingly, the partial and full agonist-bound structures of the β-adrenoreceptors provide new insights into the dynamic role of the connections among TM3, TM5, and TM6 in the initial steps of the activation process.[17,18]

With the availability of crystal structures, there has been a renaissance of GPCR computational and structural studies. Computational techniques like molecular dynamics (MD) simulations,[26−30] protein−protein docking,[31] and virtual screening[32] have gone beyond the static crystallographic structures of the β-adrenergic receptors and have allowed for a more comprehensive exploration of the functionality of this family of GPCRs. In particular, MD simulations have provided important insights into delicate conformational changes such as the ionic lock and its microenvironment in the β-adrenergic receptors.[26−29] Additionally, computational studies of rhodopsin employing the LITiCON method,[33] prior to the release of the activated opsin structure, and recent metadynamics simulations of the same system[34] already predicted the conformational events observed in the rhodopsin activation process.

Two years after the release of the A_{2A}AR structure, some effort has been spent on this, including the identification of novel chemotypes using structure-based virtual screening,[35] the postulation of the stabilization effect of cholesterol molecules in the hA_{2A}AR,[36] and the influence of the saline concentration in the formation of the ionic lock,[30] both items studied by MD simulations on this particular receptor. Despite the importance of these initial efforts, a deeper structural and dynamic exploration of the ARs is clearly needed to gain comprehensive insight into this particular family of GPCRs. In this work, all-atom molecular dynamics simulations of the ligand-free structures of the two human A_2 receptors (hA_{2A}AR and hA_{2B}AR) are performed in a hydrated membrane model. Moreover, simulations of the A_{2A}AR evaluating different variables for further exploring the results of the apo form of the receptor are conducted, including the consideration of the cocrystallized antagonist ZM241385. With this approach, conserved motifs in the GPCR superfamily, identified by sequence[37,38] and recent comparative structural analysis,[3,39] are deeply analyzed, and their role in the conformational equilibrium of ARs is recognized. In addition to the formation of the ionic lock and the characterization of the connecting residues among transmembrane helices TM1, TM2, and TM7, we report a novel network of residues connecting TM3, TM5, and TM6 that we propose to be an important step for the activation process. The structural role of several particular residues of the AR family arises, which is discussed in the context of available experimental data.

MATERIALS AND METHODS

Residue Numbering. The general GPCR numbering scheme proposed by Ballesteros and Weinstein[40] was adopted throughout this work because it allows a proper comparison between different receptors. Briefly, every residue is labeled as *X.YY*, where number *X* corresponds to the TM helix (from 1 to 7) and *YY* is a correlative number starting from the most conserved residue in each helix (to which a *YY* value of 50 is assigned). Additionally, the absolute receptor sequence number is indicated with a

superscript when considered necessary (i.e., loop regions), following the corresponding Swiss-Prot sequences (P29274 for A_{2A}AR and P29275 for A_{2B}AR).

Molecular Modeling of Adenosine Receptors. The structure of the A_{2A}AR in a complex with its potent inhibitor ZM241385 was retrieved from the Protein Data Bank (PDB) (entry 3EML). The missing regions of the receptor were modeled by using Modeller version 9.4.[41] These include a fragment of EL2 (^{149}PKEGKNH^{155}), undetermined in the crystal structure, and the IL3 segment (^{209}KQMESQPLPGERA^{221}), which was substituted with the T4 bacteriophage lysozyme in that structure. The other two missing regions were not considered in this work, i.e., a small N-terminal fragment (^{1}MP^{2}) and the 95-residue C-terminus. Fifteen initial models of the missing regions were built. The top five models, according to DOPEHR scoring, were selected for further refinement with the LoopModel routine.[42] Thus, a pool of 10 models per input structure were generated. One model per input structure was selected again according to DOPEHR scoring, and a final selection among the five candidates was done by a combination of visual inspection and quality analysis using Procheck[43] and Molprobity.[44] The side chain conformations of all Asn, Gln, and His residues were assessed with Molprobity[44] and PDB2PQR[45] prediction servers. The Protein Preparation Wizard utility (Schrödinger LLC, New York, NY) was employed to add hydrogens and initially define protonation states of titratable residues and Ser/Thr rotamer assigments. A deeper exploration of the protonation states of Glu1.39−His7.43 and Glu^{169} (5.30)−His^{264} (7.29) residue pairs was performed with MCCE.[46] Briefly, this software generates side chain conformers for the residues under study, performs continuum electrostatics calculations with DelPhi[47] as the Poisson−Boltzmann equation solver, and performs a final titration simulation employing Monte Carlo sampling. Twelve different rotamers were generated for the aforementioned residues and those within 0.4 nm of them. A slab of neutral atoms surrounding the protein was added to mimic the effect of a cellular membrane.[48] Default parameters were employed for the rest of the directives.

A partial energy minimization of the modeled loops was performed on the selected structure with Macromodel,[49] using the Polak-Ribiere Conjugate Gradient (PRCG) with a convergence criterion of 0.05, and the OPLS2005 force field[50,51] in combination with the GBSA solvation model. The modeled regions were unrestrained, applying a positional harmonic constraint (2×10^4 kJ mol^{-1} nm^{-2}) to the rest of EL2 and any other residue within 2 Å of modeled regions, while the rest of the protein was completely frozen.

The hA_{2B}AR structure was obtained by homology modeling using Modeller with the hA_{2A}AR as a template. First, a multiple-sequence alignment of multispecies A_{2A}AR and A_{2B}AR receptors was generated with ClustalX2.0,[52] using the PAM250 substitution matrix, and open and elongation gap penalties of 10 and 0.05, respectively. In analogy with the A_{2A}AR structure, the first three residues of the N-terminus and the last 13 residues of the C-terminus were discarded for the modeling. The modeling protocol was adapted from that employed by some of us in the GPCRdock2008 competition:[53] 15 initial models were obtained using standard Modeller parameters, selecting the top five models on the basis of the DOPEHR scoring function to be further refined by means of the Molprobity server.[44] The best model was selected using a compromise between the DOPEHR scoring and the geometrical quality assessment of Procheck and used as a starting point for a loop optimization procedure with the LoopModel routine of Modeller. Only the loop regions with no secondary structure were subjected to this refinement step (i.e., the three extracellular loops, excluding the short helical fragment ^{173}FENV^{176} of EL2, and IL3) and 15 models were generated. The final selection was performed using criteria identical to those used in the previous step: Procheck stereochemical quality and the DOPEHR energetic ranking. The addition of hydrogens, refinement, and optimization of the geometry of the loop regions using energy minimization procedures were performed as described above for the hA_{2A}AR.

Insertion into the Membrane and Molecular Dynamics Simulations. An automated protocol for the insertion of the GPCR structures into an explicit membrane model, using a combination of ad hoc Linux shell scripts and GROMACS utilities, was developed. Briefly, the protocol consists of the following steps. (i) The GPCR structure (hA_{2A} or hA_{2B}ARs in our case) is introduced into the center of a hexagonal prism-shaped box with the receptor TM helices and the box symmetry axes parallel to the z direction, with every side box walls at a minimum of 2.0 nm and every top and bottom box walls at a minimum of 0.8 nm of any atom. (ii) A hydrated POPC gel-phase bilayer with exactly the same dimensions as the box of the previous step, with the hydrophobic phase parallel to the $x-y$ plane and located at half of the z dimension, is created from a larger bilayer preequilibrated at 260 K, just by removing the excess of lipid and water molecules. (iii) The resulting bilayer was copied on the receptor box. (iv) The water and lipid molecules overlapping any protein atom were removed. (v) Cl^- ions are introduced to neutralize the total charge of the receptor at physiological pH (from 6 to 12, depending on the receptor and protonation state considered for the histidine residues). The abovementioned gel phase instead of a liquid-crystalline bilayer was employed to optimize the packing of lipids around the AR model. The final systems consist of approximately 14000 water and 200 lipid molecules, in addition to the Cl^- ions and the receptor structure.

MD simulations were performed by applying the recently published half-ε double-pairlist method[54] to make compatible the so-called Berger united atom parameters[55,56] used for the lipids with the OPLS-AA force field[50,51] employed for the receptor and ions. Simple point charge (SPC) water molecules[57] were included to solvate the systems. All the simulations were performed using periodic boundary conditions in the three spatial dimensions with hexagonal prism-shaped boxes. This geometry allows us to optimize the use of the solvent with respect to the rectangular prism, by saving 13.4% of the volume for the same distance to the periodic images, and to increase the isotropy of the unavoidable interaction of the receptor with its periodic images. A semiisotropic Parrinello-Rahman barostat[58,59] was employed to maintain the pressure independently in the $x-y$ plane and in the z direction at 1 bar with a coupling constant of 2 ps. The isothermal compressibility constant was 4.5×10^{-5} bar^{-1}. The temperature was kept constant at 310 K using a Nose-Hoover thermostat[58,59] by coupling independently the lipid molecules, the protein, and the water−ion groups with a common period of 0.1 ps. A cutoff of 1.2 nm was employed for the Lennard-Jones potential. The long-range interactions were calculated using the particle mesh Ewald method[60,61] with a 1.2 nm real space cutoff, a 0.15 nm space grid, and a fourth-order B-spline interpolation scheme to optimize the computational performance, giving a PME load of ∼25%. The initial velocities of the atoms were randomly assigned to produce a Maxwell

distribution corresponding to the temperature at which the simulation will be performed. The equations of motion were integrated using the leapfrog method[62] with a 2 fs time step. The bonds lengths and H−O−H angle in water were constrained using the SETTLE algorithm,[63] while the LINCS algorithm[64] was used to constrain bond lengths in the protein and lipid molecules. All the simulations were performed using GROMACS[65,66] version 4.0.5. Simulations of POPC lipid bilayers at different temperatures using the same parameters were performed to ensure that they reproduce the experimental area per lipid and the right deuterium order parameters.

An equilibration protocol was specifically designed for this system to avoid potential unfolding or distortion of protein regions because of a less exhaustive equilibration. This protocol is summarized in Table 1 and includes the following stages: (i) harmonic positional restrictions on all the heavy atoms of the protein to equilibrate the lipids and water molecules (five steps of 1 ns each, decreasing the force constant from 1000 to 200 kJ mol^{-1} nm^{-2}, by 200 kJ mol^{-1} nm^{-2} in each step), (ii) harmonic positional restrictions on the α-carbon atoms of the protein to equilibrate the protein side chains with the surrounding atoms (6 ns using a force constant of 200 kJ mol^{-1} nm^{-2}), (iii) harmonic positional restrictions on the α-carbon atoms of the receptor transmembrane regions to equilibrate the loops, avoiding helix perturbations (21 ns using a force constant of 200 kJ mol^{-1} nm^{-2}), and (iv) fully unrestrained simulations [100 ns for the main simulations (see Table 2)]. After the first few nanoseconds of the equilibration stage and during the whole production trajectory, the lipids are clearly in the disordered liquid-crystal phase. By means of the scripted protocols, independent replicas for several simulations (see Table 2) were performed under equivalent conditions. All coordinates were stored every 10 ps for further analysis.

MD trajectory analyses were conducted using GROMACS utilities (see the Supplementary Methods of the Supporting Information). PyMOL (http://www.pymol.org) was used to prepare all molecular images and to perform protein superpositions (*super* command, on the basis of the α-carbon traces).

Inclusion of Crystallographic Water Molecules and Ligand. We performed one simulation of the A_{2A}AR [RW1 (see Table 2 and Figure S1 of the Supporting Information)], in which selected crystallographic water molecules were explicitly included: residues 502, 504, 505, 509, 512, and 565 according to PDB entry 3EML. Addition of hydrogens and refinement of associated hydrogen bonds were performed with the *Protein Preparation Wizard*, followed by energy minimization of hydrogen atoms (rmsd convergence of 3.0 nm, using the OPLS2005 force field in Macromodel).

The necessary parameters needed for the crystallographic ligand ZM241385 in the OPLSAA force field were automatically obtained with Macromodel[49] and translated to the GROMACS syntax using an ad hoc script. Two MD simulations of the A_{2A}AR−ZM241385 complex [RL1 and RL1′ (see Table 2)] were conducted.

The same equilibration protocol as in the case of the apo form of the receptor was employed for these simulations, applying the same restraints to the ligand and water molecules as in the case of the side chains of the receptor.

Table 1. Description of the Equilibration Protocol and Production Stages Performed in the Simulations of AR Models in POPC Bilayers

stage	positional harmonic restrictions	comments	time (ns)
i	on all the receptor heavy atoms	five steps with decreasing force constants from 1000 to 200 kJ mol^{-1} nm^{-2}; the aim is to relax the receptor environment	5 × 1
ii	on the receptor α-carbon atoms	to relax the receptor side chains	6
iii	on the receptor α-carbon atoms of transmembrane regions	to relax the loops	21
iv	none	production trajectory	100[a]

[a] Value for the main simulations, see Table 2 for details.

RESULTS

Molecular Modeling. On the basis of the high degree of sequence similarity between the two human A_2ARs (59 and 70% for the whole protein and the TM domains, respectively), the crystallographic structure of the hA_{2A}AR was employed as a template to produce a homology model of the hA_{2B}AR. As expected, the main topological features of the TM region are common to both structures, the most important divergent sequences being located in the longest loops. The topology of EL2 is influenced by the four additional residues in the A_{2B}AR (37 vs 33 residues in the A_{2A}AR) and by the different arrangement of the three disulfide bonds, which were assigned to the A_{2B}AR on the basis of a family sequence alignment (data not shown). Two disulfide bridges are conserved between both receptors: the first one connects EL1 and EL2 (residues 71−159 in the A_{2A}AR and residues 72−167 in the A_{2B}AR), whereas the second one is the highly conserved disulfide bridge in the GPCR superfamily, located between EL2 (residue 166 in the A_{2A}AR and residue 171 in the A_{2B}AR) and TM3 (position 3.25).

Table 2. Description of the Performed Simulations, Together with the Longitudes of Their Production Phases

code(s)	description	simulated receptor	production time (ns)
R1, R2	receptor with a residue at position 7.29 in its neutral form, replicas 1 and 2	A_{2A}AR, A_{2B}AR	100
R1′, R2′	receptor with residue His7.29 in its charged form, replicas 1 and 2	A_{2A}AR	90
R1″	receptor with both residues His7.29 and His7.43 in its charged form	A_{2A}AR	90
RW1	receptor with crystallographic water molecules	A_{2A}AR	90
RL1	receptor as in R1, R2, in complex with the crystallographic ligand	A_{2A}AR	30[a]
RL1′	receptor as in R1′, R2′, in complex with the crystallographic ligand	A_{2A}AR	50

[a] This MD simulation was not extended until 50 ns because of the high instability of the complex under these conditions.

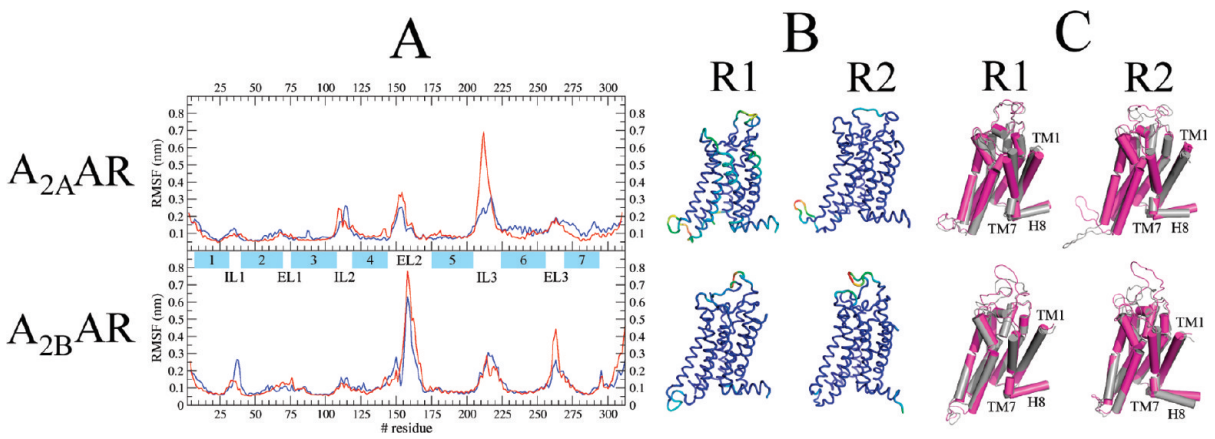

Figure 1. Dynamic properties of simulated A_2ARs. (A) Root-mean-square-fluctuation (RMSF) for each receptor under study (A_{2A}AR, top; A_{2B}AR, bottom). In each case, the blue line stands for the R1 replica and the red line accounts for replica R2. Cyan boxes denote the location of the TM helices. (B) For each MD simulation (R1, left; R2, right; A_{2A}AR, top; A_{2B}AR, bottom), the reference structure used for rmsf calculations (see the text) is represented in ribbons and colored by the gradient of the estimated β factors (from blue to red, which indicates the highest mobility). (C) Graphical representation of the PCA. The two extreme projections on the first eigenvector are represented with silver and magenta cartoons. The extracellular part of TM1 and the intracellular side of TM7 are labeled (together with C-terminal helix 8, H8). The rest of the TMs are ordered in a counterclockwise direction. The results from the different MD simulations are arranged as in panel B.

However, a third cysteine bridge is present in each receptor between nonconserved positions within the family: in the A_{2A}AR this connection is established between EL2 (residue 146) and the tip of TM3 (position 3.22), offering an additional conformational constraint to the loop, while in the A_{2B}AR the bridge is established between positions 154 and 166 in EL2. With respect to IL3, the modeled conformations are relatively extended in the two receptors, being four residues longer in the A_{2A}AR (17 vs 13 residues in the A_{2B}AR). It must be noted that IL3 has been identified as an unstructured region in GPCRs;[14] thus, the model quality of this region is very limited because of the absence of the cognate G protein. Finally, a fourth disulfide bridge constrains particularly the structure of EL3 in the A_{2A}AR. This bridge, located between positions 259 and 261, is not totally conserved in the AR family, being absent in the A_{2B}AR. An interaction between EL3 and EL2 is established through polar interactions of the side chains of Glu5.30 in EL2 (conserved in both A_{2A}AR and A_{2B}AR) and position 7.29 in EL3, occupied by His^{264} in the A_{2A}AR or Asn^{266} in the A_{2B}AR.

Geometrical and Conformational Analysis of MD Simulations. The structures obtained for the two hA_2ARs were employed as starting conformations for extensive MD simulations in an atomistic model of the membrane. Because of the crystallization conditions of the A_{2A}AR, bound to the ZM241385 antagonist, starting conformations of the two receptors should be considered to be in the inactive state. Most MD trajectories here discussed were obtained in the absence of any ligand, in an attempt to observe the initial stages of the activation conformational pathway, which was recently suggested in the case of the β2-adrenergic receptor.[28] This strategy is further supported by the fact that constitutive activity was described for the A_{2A}AR.[67,68] Furthermore, the influence of the antagonist ligand in the dynamic behavior of the A_{2A}AR was also examined (see below). To efficiently sample the conformational space and to check for reproducibility of the main structural features, two independent replicas with different random seeds were conducted for each receptor [from now on simulations R1 or R2 for either the A_{2A}AR or the A_{2B}AR, respectively (see Table 2)]. Taking into account the fact that the entire A_{2B}AR structure as well as part of the A_{2A}AR was modeled, we took special care during the equilibration process, which was sufficiently long to allow the progressive relaxation of solvent molecules, loop residues, and TM regions. The 100 ns long production stage started well after a plateau for the root-mean-square deviation (rmsd) of the loops was reached (see Figure S2 of the Supporting Information). Unless the contrary is stated, the rest of the analyses will refer to the unrestrained production phase of each replica.

The backbone rmsds of the whole receptors fluctuate, as a function of time, within the values typically obtained for protein crystal structures, between 0.2 and 0.4 nm (see Figure S2 of the Supporting Information). The root-mean-square fluctuation (rmsf) values per residue (Figure 1) were determined using the most representative protein conformation as the reference structure, which was obtained by cluster analysis of each trajectory (see the Supplementary Methods of the Supporting Information). The regions with the highest mobility for the A_{2A}AR were found to be IL3, EL2, and IL2. For the A_{2B}AR, EL2 seems to be by far the most mobile region in the two replicas, followed by EL3 and IL3. The reason for the higher flexibility of EL2 in the A_{2B}AR must be found in the different arrangement of the disulfide bond in this loop: in this receptor, the disulfide bond occurs between two cysteine residues located within EL2, which consequently has more conformational freedom, whereas in the A_{2A}AR, this bond connects EL2 to the end of TM3, thus restraining the movement of the loop. The rmsf results fit well with the experimental data available for the A_{2A}AR crystal structure, because it is precisely the unsolved tip of EL2 (residues 149−155) showing the largest fluctuations (Figure 1A,B). Also in the extracellular region, EL3 shows a higher mobility in the A_{2B}AR, likely because of the lack of the particular disulfide bond occurring within EL3 in the A_{2A}AR.

With regard to the intracellular loops, the use of the T4L fusion protein strategy in the crystallization process accounts for the highly unstructured nature of IL3 in the GPCRs.[14] This is in good agreement with the rmsf results shown in Figure 1, in

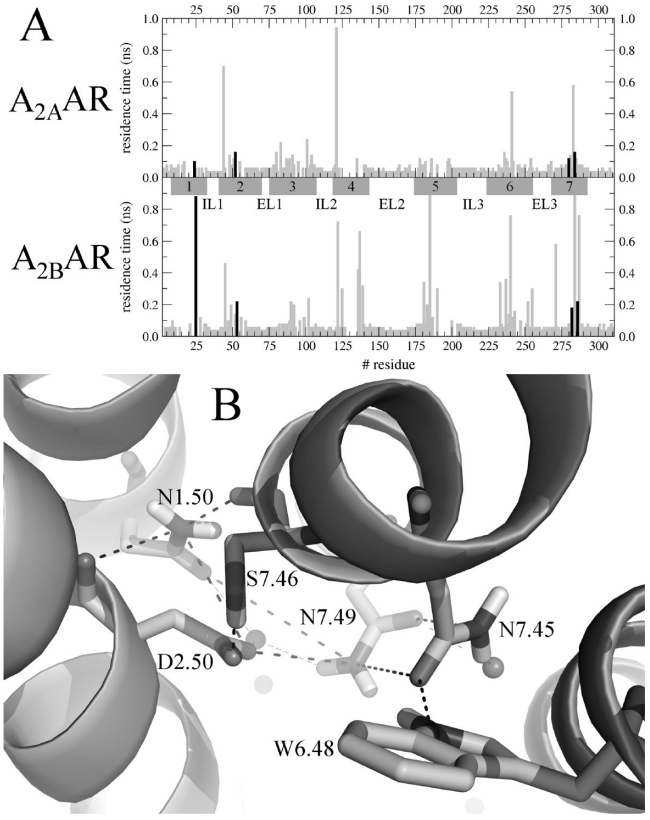

Figure 2. Water analysis of the trajectories of A_2ARs. (A) The residence time of water molecules is represented as a function of the receptor sequence (top, A_{2A}AR; bottom, A_{2B}AR). Residence time was estimated as defined in ref 72. Residues Asn1.50, Asp2.50, Asn7.45, and Asn7.49, interacting with water molecules in the crystal structure of the A_{2A}AR, are highlighted with black bars. Dark gray boxes indicate the location of the TM helices. (B) Insight into the hydrogen bond network connecting helices TM1, TM2, TM6, and TM7 based on the crystal structure of the A_{2A}AR. The residues involved are labeled and shown as sticks, with potential hydrogen bonds depicted as dashed lines and crystallographic waters as spheres. The corresponding hydrogen bond frequencies are listed in Table 3.

particular for the A_{2A}AR, which presents the longest IL3 segment. In contrast, the relatively low rmsf of IL2 agrees with the presence of a α-helical secondary structure in this loop, and the stabilizing interactions between Tyr3.60 in IL3 and the DRY motif in the intracellular tip of TM3. Such behavior was previously observed in MD studies of β1- and β2-adrenergic receptors.[27]

Concerted motions of different domains were identified by principal component analysis (PCA) independently performed on each trajectory (see the Supplementary Methods of the Supporting Information). The extreme structures of the most representative collective motion are shown in Figure 1C, illustrating again the weight of the unstructured loop movement in the protein dynamics. Unexpectedly, the extreme conformations show that, mainly for the A_{2A}AR, TM1 and TM7 slightly separate from each other during the MD trajectories. As discussed below, this movement could be directly related to the disruption of the interaction, initially present in the crystal structure of the A_{2A}AR, between the highly conserved residues in ARs, Glu1.39 and His7.43.

Interactions with the Solvent. The previously presented set of MD simulations avoids the a priori consideration of any water molecule derived, e.g., from crystallographic observations. This was done to allow a direct comparison between the crystallographic structure of the A_{2A}AR and the homology-derived model of the A_{2B}AR, lacking such information, as it is common in most of the GPCRs of pharmacological interest. Nevertheless, a detailed analysis of the interaction of water molecules with the receptor was performed to ensure a correct behavior of the system, because water molecules have been assigned a role in the structure of GPCRs, and even in the receptor activation process.[69−71] As a first approach, the maximal residence times in the first hydration shell of every residue (i.e., water molecules a maximum distance of 0.4 nm from the given residue) were estimated as defined by Freites et al.[72] (see Figure 2A). Remarkably, the cluster of residues connecting TM1, TM2, and TM7, which interact with crystallographic water molecules in the hA_{2A}AR structure (see Figure 2B and next section), show residence times higher than the average in the two receptors, indicating that the absence of such crystal water molecules in the starting structure was successfully restored during the equilibration phase. On the other hand, most of the longest residence times correspond to residues on the intra- or extracellular edges of the helices, where water molecules are not likely to play a structural role.

Table 3. Hydrogen Bond Frequencies in the Structural Motifs Depicted in Figures 2, 5, and 6

	A_{2A}			A_{2B}	
hydrogen bond[a]	R1	R2	RW1	R1	R2
TM1−TM2−TM6−TM7[b] (Figure 2)					
N1.50−S7.46	81.91%	70.88%	67.93%	70.67%	42.95%
N1.50−D2.50	0.64%	0.84%	3.17%	6.79%	2.86%
D2.50−S7.46	72.96%	99.53%	99.04%	59.05%	48.40%
D2.50−N7.49	20.66%	95.06%	66.18%	68.22%	90.26%
N7.45−N7.49	3.15%	4.33%	0.16%	6.68%	0.00%
N7.45−W6.48	0.00%	0.00%	0.03%	0.00%	0.00%
N1.50−N7.49	0.29%	0.30%	0.00%	0.85%	4.58%
average pairs[c]	1.80	2.71	2.37	2.12	1.89
Ionic Lock[d] (Figure 5)					
D3.49−R3.50[e]	100%	100%	99.99%	97.31%	99.80%
E6.30−R3.50[e]	70.71%	99.38%	81.51%	99.38%	98.86%
D3.49−Y3.60	99.10%	81.50%	99.81%	99.88%	99.92%
D3.49−T2.39	93.06%	99.36%	99.66%	61.25%	99.88%
average pairs[c]	3.63	3.80	3.81	3.58	3.98
Toggle Switch[f] (Figure 6)					
H6.52−N5.42	8.78%	1.25%	38.80%	12.11%	40.61%
H6.52−N6.55	4.11%	0.01%	0.19%	1.43%	2.20%
Q3.37−C5.46	94.22%	83.56%	24.52%	79.96%	95.46%
Q3.37−N5.42	4.36%	0.01%	3.11%	62.01%	12.59%
average pairs[c]	1.11	0.85	0.67	1.56	1.51

[a] Hydrogen bonding frequency computed with the g_hbond utility in GROMACS, using the default parameters (cutoff acceptor−donor−hydrogen angle of 30°, cutoff acceptor−donor radius of 0.35 nm). [b] See Figure 2 for a representation of the polar interactions depicted here. [c] The average number of simultaneous hydrogen bonds per snapshot in the given motif along the MD trajectory. [d] See Figure 5 for a representation of the polar interactions depicted here. [e] See Figure 6 for a representation of the polar interactions depicted here. [f] The occurrence of the salt bridge was analyzed as a regular hydrogen bond.

dx.doi.org/10.1021/bi200100t |*Biochemistry* 2011, 50, 4194–4208

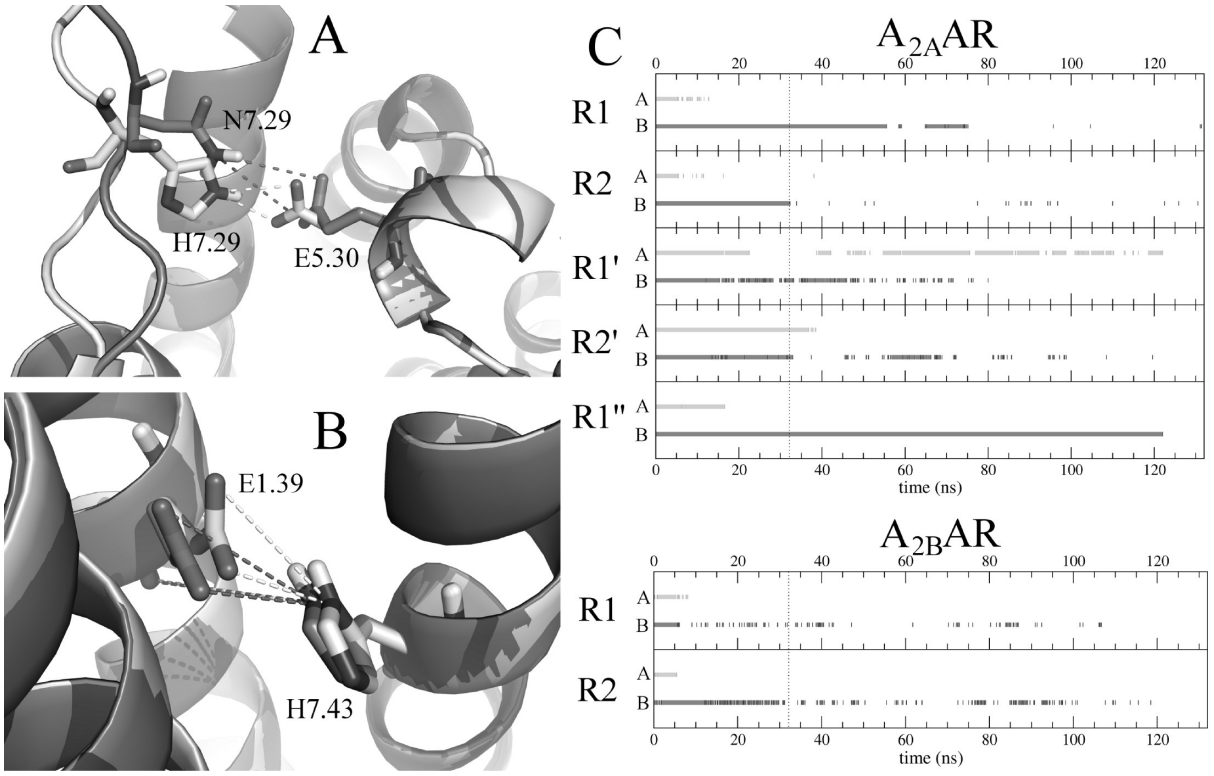

Figure 3. Interactions of specific residues of ARs. (A) Initial interaction between Glu5.30 in EL2 and the residue in position 7.29 in EL3: His^{264} in $A_{2A}AR$ (white) or Asn^{266} in $A_{2B}AR$ (gray). (B) Initial interaction between the side chains of Glu1.39 and His7.43 based on the crystal structure of the $A_{2A}AR$ (white) and the homology-derived model of the $A_{2B}AR$ (gray). (C) Hydrogen bonds between Glu5.30 and His- or Asn7.29 depicted in panel A (gray bars) and between Glu1.39 and His7.43 as depicted in panel B (black bars). Results for whole trajectories are shown; the vertical dotted line separates equilibration from the production phase. In the $A_{2A}AR$, R1 and R2 refer to replicas of the receptor with His^{264}(7.29) in neutral form; R1′ and R2′ are receptors with His^{264}(7.29) protonated, and R1″ presents both His^{264}(7.29) and His7.43 in TM7 protonated. In the case of charged histidines, both Nδ1 and Nε2 atoms are considered for the computation of hydrogen bonds with the counterpart residue.

To further confirm the feasibility the current protocol ignoring the crystallographic water molecules, we provide an additional MD simulation of the $A_{2A}AR$, including selected crystallographic water molecules [RW1 (see Table 2)]. The results are summarized in Table 3 and in Figures S1 and S2 of the Supporting Information. We can appreciate that the dynamic properties and the behavior of all structural events analyzed in this work do not significantly deviate from the behavior observed in the other two MD replica simulations of the $A_{2A}AR$. The frequency of hydrogen bonds of residues connecting TM1, TM2, TM6, and TM7 is particularly conserved, being depicted in Table 3 and discussed in more detail in the next section. A supplementary analysis of all the residues showing polar contacts with the crystallographic water molecules in the $A_{2A}AR$ points in the same direction. The bar graphs in Figure S1 of the Supporting Information represent the number of times that a residue has been ligated to a water molecule for at least 4 ns along the MD trajectories, showing the weak effect that the inclusion of the crystallographic water molecules in the equilibration protocol has on the hydration of the affected residues.

The GPCR-Conserved Hydrogen Bond Network among TM1, TM2, TM6, and TM7. In the crystal structure of the $hA_{2A}AR$, transmembrane segments TM1, TM2, TM6, and TM7 interact through a GPCR-conserved hydrogen bond network (Figure 2B), which is putatively important in maintaining the architecture of the heptahelical bundle and for the activation mechanism of GPCRs.[73,74] This network is formed by the following elements, where the percentage of conservation in the GPCR class-A family[38] is indicated in parentheses. The side chain of Asn1.50 (100% conserved) interacts with the backbone of Ser7.46 (63%), the side chain of which interacts with Asp2.50 (94%). A water molecule mediates hydrogen bond interactions among Asp2.50, Asn1.50, and Asn7.49 (75%). Finally, a second water molecule connects the last residue with Asn7.45 (67%), which at the same time is directly hydrogen bonding to Trp6.48 (71%), the so-called toggle switch residue.

The analysis of such a hydrogen bond network, summarized in Table 3, shows the stability of the interactions among residues Asn1.50, Ser7.46, Asp2.50, and Asn7.49. All the involved residue pair hydrogen bonds register high frequencies in R1, R2 replicas of both receptors, and in simulation RW1, with an average number of two simultaneous hydrogen bonds. Interestingly, the complexity of this hydrogen bond network was recently revealed by the recent exploration of the protonation state of Asp2.50 in the β-adrenergic receptors[75] or by the influence of sodium ions in a recent MD simulation of a model of the D_2 dopamine receptor.[76]

It is worth attending to the time evolution of residue Asn7.45. In the crystal structure of the $A_{2A}AR$, the oxygen in the side chain of this asparagine is hydrogen bonding to the side chain of Trp6.48. This interaction had been predicted by structural comparison of GPCR models with the crystal structure of rhodopsin, in which the lack of Asn at position 7.45 is supposed to be counterbalanced by crystallographic water molecules mediating interaction with Trp6.48, which is this way arrested

in the *gauche*+ (*g*+) rotamer.[70] However, in the crystal structures of the β-adrenergic receptors, the rotamer of Asn7.45 appears to be flipped with respect to the crystallographic position of this residue in the $A_{2A}AR$, thus avoiding such interaction with Trp6.48. Our MD simulations of both ARs are in agreement with this last experimental observation, because a change in the rotamer of Asn7.45 has already been registered in the equilibration process of all five simulations (Figure S3 of the Supporting Information), leading to the disruption of the hydrogen bond postulated in the crystal structure of the $A_{2A}AR$.

Interactions between Specific Residues of the Adenosine Receptor Family. Besides residues conserved in the rhodopsin-A class of the GPCR superfamily, some particular positions of the AR family members deserve special attention, to elucidate their potential structural role.

One particular interaction of the $A_{2A}AR$ crystal structure connects extracellular loops EL2 and EL3 (Figure 3A). In this structure, where the receptor is in complex with the antagonist ZM241385, Glu5.30 (EL2) accepts two hydrogen bonds: one coming from the amino group in the ligand and another coming from His^{264} (position 7.29) in EL3 making this loop act as a lid that closes the binding site stabilizing the complex (see Figure 4A). Such a role of the ELs in the ligand entrance has been hypothesized in recent molecular modeling of ARs.[77] In the $A_{2B}AR$ model presented here, the role of this histidine is played by Asn^{266} (see the multiple-sequence alignment of EL3 of the human ARs in Figure S4 of the Supporting Information), which seemed to point out that a polar interaction, rather than a salt bridge, would be conserved between the two loops. This possibility was not discarded by the pK_a prediction of PDB2PQR, which assigns the neutral form for His7.29 (pK_a = 7.03), which we subsequently considered in the first instance for our simulations (replicas R1 and R2 of the $A_{2A}AR$). However, such interaction is broken in the equilibration phase of two replicas simulated per receptor (Figure 3C), a result that would lead to the hypothesis that in the apo form of the receptor, this interaction is easily broken to allow access of extracellular diffusible molecules to the binding site. On the other hand, further ionization state calculations with MCCE predicted His7.29 with a net positive charge, which encouraged us to simulate two independent replicas of the apo state of the $A_{2A}AR$ considering this residue charged. As one can see in Figure 3C (R1′ and R2′), the interaction initially maintained between EL2 and EL3 through a salt bridge between His7.29 and Glu5.30 is frequently observed (61% of the time) in R1′, while in R2′ the frequency of this interaction is only slightly higher (6%) than in the cases where His7.29 was modeled neutral (0% occurrence). Because it is not clear from the simulations whether in the apo state this histidine is positively charged, the next step was to investigate whether a charged histidine could favor the closed state of the extracellular loops as observed in the crystal structure of the $hA_{2A}AR$ in complex with an antagonist (Figure 4A). Subsequent MD simulations of the $A_{2A}AR$ in the presence of the ligand were performed. Here, a neutral His7.29 in EL2 [simulation RL1 (Table 2)] promotes an opening of the lid formed by EL2 and EL3, resulting in the loss of most receptor–ligand interactions (see Figure 4B, top panel). On the other hand, a charged histidine in that position [simulation RL1′ (Table 2)] maintains such a lid atop the ligand and the complex remains stable for the rest of the simulation (Figure 4B, bottom panel), thus pointing out a preference for the protonated state of this histidine in the holo form of the receptor.

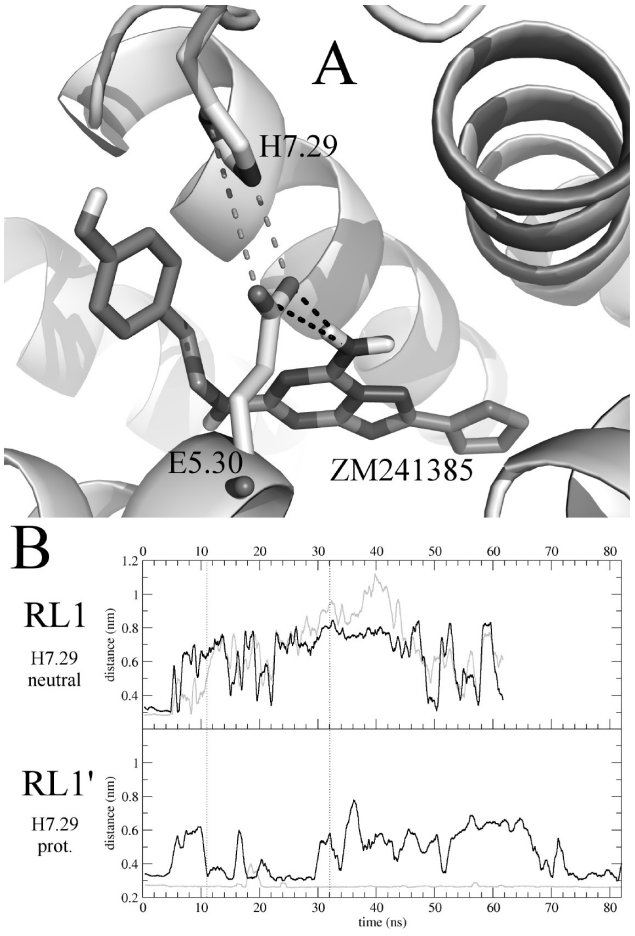

Figure 4. Influence of the protonation state of His^{264}(7.29) in the dynamics of the crystallographic protein–ligand complex. (A) Representation of the initial structure of the $A_{2A}AR$ (white) in complex with ZM241385 (gray). Key residues are labeled. (B) Measurement of the minimum distances between Oε atoms of Glu5.30 and (i) the nitrogen of the ligand's exocyclic amino group (black lines) and (ii) the Nδ1 and Nε2 atoms of His7.29 (gray lines), as depicted by dashed lines in panel A. Results of whole trajectories are shown, with vertical dotted lines indicating the release of the positional restraints for the ligand (11 ns) and the release of restraints for the α-carbon atoms in the loops (32 ns).

We also focused on two residues completely conserved in the ARs family: a glutamic acid in position 1.39 and a histidine in position 7.43, which are close in space in the $A_{2A}AR$ crystallographic structure and had been previously postulated to interact through a hydrogen bond.[78−80] To initially form such a hydrogen bond (Figure 3B), the histidine residue was protonated at Nδ, as suggested by several of the considered prediction tools (Schrödinger, Molprobity, and PDB2PQR), even though the geometry of the hydrogen bond in the crystal structure is not associated with a strong interaction, taking into account the ideal geometries derived from the study of the Baker group[81] [θ angle = 99°; ψ angle = 88°; δ_{HA} = 0.25 nm (see the original reference for details of these values)]. Accordingly, MD simulations with His7.43 in its neutral form show that this hydrogen bond tends to be transient or even completely broken, only being significantly occupied (27%) in R1 of the $A_{2A}AR$, but with an occupancy of <8% in the remaining simulations, including both replicas of the $A_{2B}AR$ (Figure 3C). It is worth noting that His7.43 has been experimentally involved

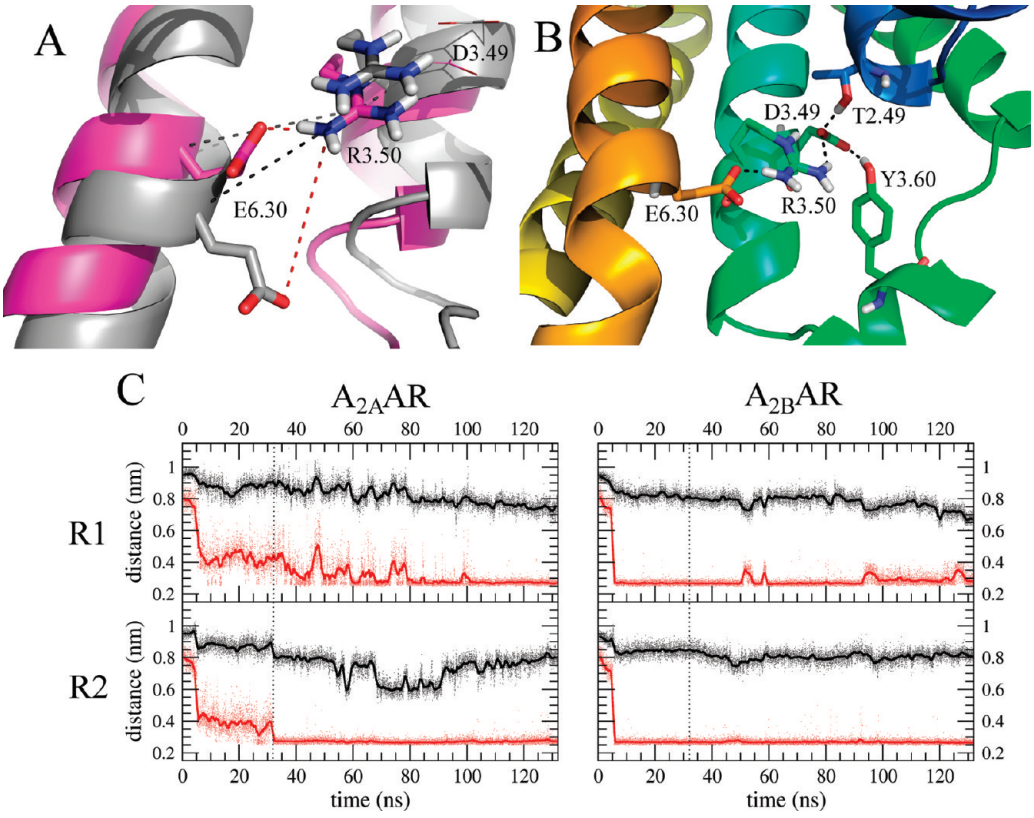

Figure 5. Analysis of the ionic lock. (A) Salt bridge between Arg3.50 and Glu6.30, commonly termed the ionic lock, in the A_{2A}AR. The initial configuration (gray) and a stable snapshot (magenta) are superimposed. (B) Representative snapshot of the hydrogen bond network in which the ionic lock is contextualized. The residues involved in helices TM2 (cyan), TM3 (green), and TM6 (orange) are labeled and shown as sticks, with potential hydrogen bonds depicted as dashed lines. The corresponding hydrogen bond frequencies are listed in Table 3. (C) For R1 and R2 of both receptors, the time evolution of the minimum distance between any Oε atom of Glu6.30 and any Nζ atom of Arg3.50 is colored red (thick line representing the smoothed version). Similarly, the corresponding distance between the α-carbons of the same residues is represented in black. Results for whole trajectories are shown; the vertical dotted line separates equilibration from the production phase.

in agonist binding,[82] presumably through interaction with the hydroxyl groups of the ribose ring of those ligands. It remains unclear whether the proposed agonist−receptor interaction should occur through hydrogen bond acceptance of Nε of His7.43 (meanwhile, its Nδ interacts with Glu1.39[80]) or whether this interaction with the agonists promotes a disruption of the hydrogen bond with the adjacent Glu1.39. In Figure 3C, the fact that this interaction is spontaneously broken in the absence of any ligand can be appreciated, thus suggesting an important role of this residue in the conformational equilibrium of the receptor,[78] probably connected with the structural changes described above for TM7 (Figure 1C). Conversely, a salt bridge interaction is strongly suggested by the pK_a calculations performed with MCCE on this pair of residues. This possibility was considered in an independent MD simulation of the A_{2A}AR, where both His7.29 and His7.43 are modeled in their charged form, from now on simulation R1″. Figure 3C shows how the established salt bridge of a positively charged His7.43 with Glu1.39 is sufficiently strong to maintain a tight interaction between TM1 and TM7. Accordingly, the separation of TM1 and TM7 is not observed in a PCA analysis of this replica (Figure S5 of the Supporting Information), as opposed to what is shown in Figure 1 when the His7.43 is modeled in its neutral form. Alternate protonation states, such as a protonated form of Glu1.39, were not suggested by any of the pK_a prediction software used.

Ionic Lock. The TM3−TM6 ionic lock, linking the (D/E)RY motif in TM3 with Glu6.30 in TM6, is broken in the crystal structure of the A_{2A}AR, which happened in the β1- and β2-adrenergic receptor crystal structures and in contrast to what was expected in an inactive form of a GPCR.[23] As one can appreciate in Figure 5, the ionic lock is achieved in main simulations performed on both A_{2A}AR and A_{2B}AR receptors (replicas R1 and R2). In the A_{2A}AR, this interaction is formed at the end of the equilibration phase (R2) or even after 50 ns of the production phase (R1), while in both replicas of the A_{2B}AR, the lock is formed just after a few nanoseconds of equilibration time. In all four cases, once the lock is formed it can be considered strong and stable for the rest of the simulation time (see Table 3). It is also important to note that in all these cases TM3 and TM6 approach each other, as measured by a decrease in the distance between the α-carbons of Glu6.30 and Arg3.50 (Cα−Cα distance, comparing the initial value with the averaged distance of the last 20 ns, reduced in a magnitude by 0.137 to 0.232 nm, depending on the replica). The whole network of polar interactions is depicted in Figure 5B and quantified in Table 3. Such interactions involve not only salt bridges between Arg3.50 and both Asp3.49 and Glu6.30 but also stable hydrogen bonds between Asp3.49 and Tyr3.60 in IL2 and Thr2.39 in TM2. This particular network around Asp3.49, with almost four simultaneous interactions as an average, might be responsible of the strong salt

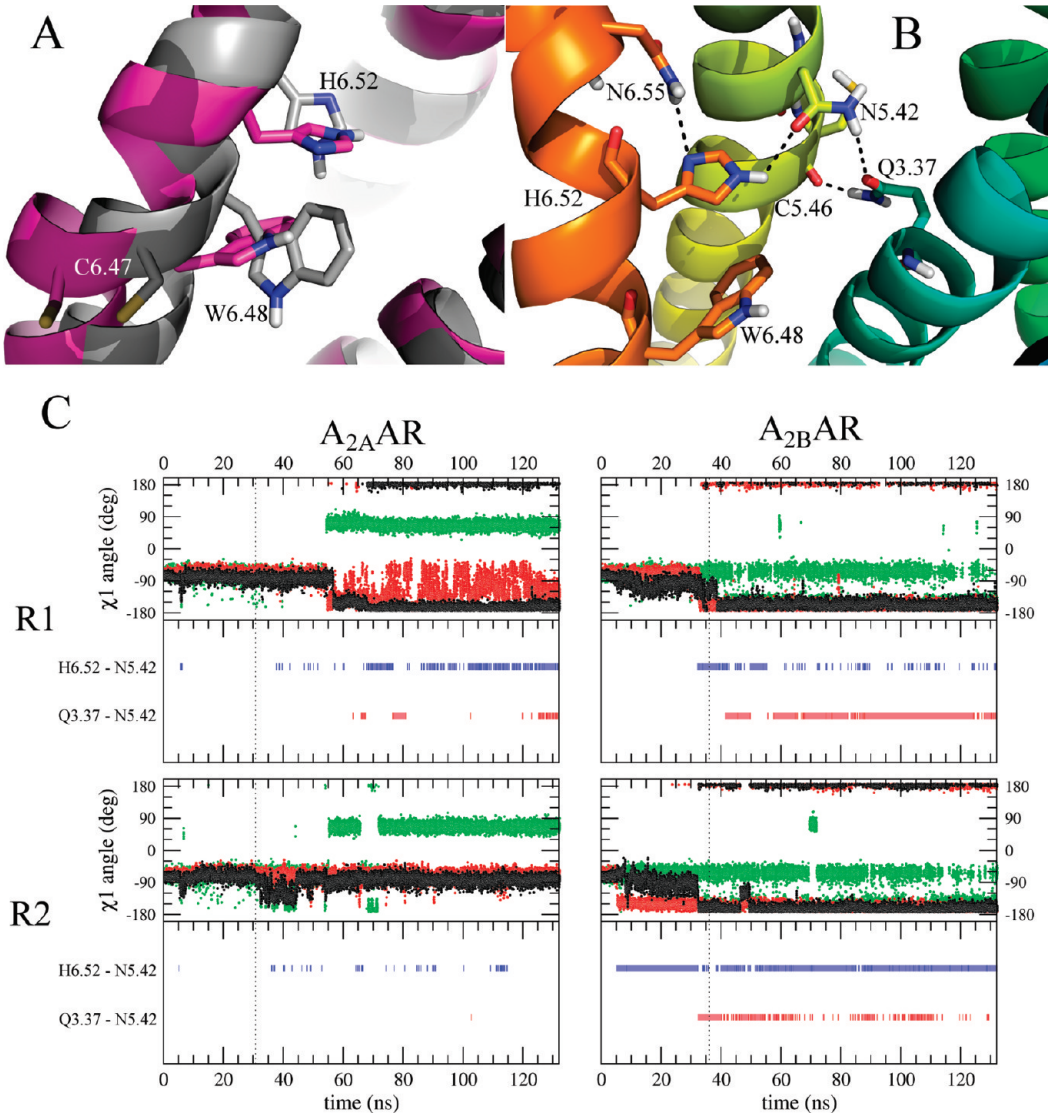

Figure 6. Analysis of the toggle switch. (A) Initial phase (gray) and a stable snapshot of the production phase (magenta) of the side chain configuration of residues Cys6.47, Trp6.48, and His6.52, showing the formation of the so-called toggle switch in the A_{2A}AR. (B) Three-dimensional representation of the potential hydrogen bonds (dashed lines) between the residues surrounding the toggle switch (sticks), located at helices TM3 (cyan), TM5 (yellow), and TM6 (orange). The corresponding hydrogen bond frequencies are listed in Table 3. (C) A separate panel for each MD simulation represents the time evolution of the χ_1 dihedral angles of the residues involved in the toggle switch (top part): Trp6.48 (black dots), His6.52 (red dots), and Cys6.47 (green dots). The bottom part of each panel represents the evolution of the hydrogen bonds of Asn5.42 with His6.52 (blue bars) or with Gln3.37 (red bars). Results of whole trajectories are shown; the vertical dotted line separates equilibration from the production phase.

bridge of this residue with the adjacent Arg3.50, which has been proposed as the primary constituent of the ionic lock by Vogel et al.[21]

Conformational Changes Accompanying the Toggle Switch. The conformational changes associated with the GPCR conserved motif, (6.47)CWxP(6.50), have been thoroughly examined in the A_{2A}AR and A_{2B}AR structures (Figure 6). The χ_1 dihedral angles of selected residues were recorded along the different MD simulations. The starting rotameric state of Trp6.48 in both receptors corresponds to the $g+$ rotamer ($\chi_1 \sim -80°$), which is associated with the inactive conformation. On the other hand, the toggle switch is considered active when this residue adopts a *trans* (t) conformation; i.e., the χ_1 dihedral is in the equivalent regions defined between $-120°$ and $-180°$ or between $120°$ and $180°$.[22] This rotameric transition might be concerted with conformational changes in positions 6.52 and 6.47, as described in the β2-adrenergic receptor.[22] Position 6.52 is frequently an aromatic residue in class-A GPCRs (82% Phe), while position 6.47 is a Cys in 74% of the cases.[38] Whereas the last residue is conserved in the two A_2AR subtypes, the former is occupied by a histidine in all ARs members, with the exception being the A_3AR, where a serine is present. In the crystal structure of the A_{2A}AR, both His6.52 and Cys6.47 show approximately the same χ_1 angle as residue Trp6.48 (i.e., $g+$ conformation). As depicted in Figure 6, we observe the transition of the toggle switch in R1 of the A_{2A}AR (after 24 ns in the production phase) and in the two replicas of the A_{2B}AR (where the change occurs just after the equilibration phase). In all four cases, there is a clear correlation between the rotameric states of the toggle switch (Trp6.48) and residue His6.52, because the last also suffers a

transition from the $g+$ rotamer to the t rotamer only when the toggle switch changes its conformation. Remarkably, in R2 of the $A_{2B}AR$, the conformational change in His6.52 clearly precedes the formation of the toggle switch, suggesting that the rotameric change of the aromatic residue in position 6.52 (His in the ARs considered here) might favor the formation of the toggle switch. In R1 of the $A_{2A}AR$, the t conformation of His6.52 prevails 59% of the time after the irreversible formation of the toggle switch, which occurs simultaneously with the conformational change of His6.52. On the other hand, the toggle switch does not occur in R2 of the $A_{2A}AR$ along the simulated time, and consequently, the rotamer of His6.52 stays in the native $g+$ state. Finally, we have investigated the possible correlation between the toggle switch and the rotameric state of Cys6.47, as previously suggested on the basis of molecular modeling of the β2-adrenergic receptor.[22] We observe that, in the $A_{2A}AR$ simulations, Cys6.47 changes its rotameric state in both R1 and R2 simulations, while the toggle switch occurs in only R1. On the other hand, Cys6.47 does not change its conformation in any of the two simulations of the $A_{2B}AR$, where the toggle switch invariantly occurs. Thus, our simulations do not support a correlation of the rotameric state of Cys6.47 with the formation of the toggle switch.

It is important to note the interactions of His6.52 with Asn5.42 in TM5 through a side chain hydrogen bond, which is somehow concerted with the rotameric state of the former residue in TM6. The complete hydrogen bond network, which also involves residues in TM3, is depicted in Figure 6B and quantitatively analyzed in Table 3. It can be appreciated in Figure 6C that His6.52 needs to adopt the t rotameric state to form the hydrogen bond with Asn5.42. As a consequence, the frequency of this hydrogen bond is significant only in the three cases when the toggle switch is formed (i.e., all cases except R2 in the $A_{2A}AR$), although only in one case (R2 of the $A_{2B}AR$) can this interaction be considered stable. It is worth noting that Asn6.55, which is crucial for the ligand binding,[12] does not form any stable interaction with the residues in the vicinity in the MD simulations (performed in the absence of any ligand). In particular, the possibility of an interaction with His6.52, located almost one α-helix turn below, is not feasible according to the data presented in Table 3. On the other hand, Asn5.42 tends to form a hydrogen bond with Gln3.37 once the toggle switch is formed. Gln3.37 also strongly connects to TM5 through a hydrogen bond with the main chain of Cys5.46 (Figure 6B and Table 3). The consideration of the crystallographic water molecules on the $A_{2A}AR$ MD simulation (RW1, with W565 in the vicinity of the aforementioned residues) results in only subtle effects on the identified network: the interaction between TM6 and TM5 (His6.52 and Asn5.42) is more prominent, whereas the interaction between TM5 and TM3 (Cys5.46−Gln3.37) is somehow weakened as compared to the MD simulations without any crystallographic waters.

DISCUSSION

The release of the $hA_{2A}AR$ structure in an inactive conformation offers an excellent starting point for a deep exploration of the conformational and dynamic properties of the adenosine receptor family. In this work, we have studied the two human A_2 receptors ($hA_{2A}AR$ and $hA_{2B}AR$) through all-atom MD simulations, generating independent replicas for each receptor. This schema allows extraction of more robust conclusions than if only one replica per receptor were performed, even if the duration of the simulation would be longer. Overall, a general analysis of the MD trajectories shows good agreement with the expected behavior of a GPCR, with higher mobility of the loop regions, while TM segments remain more stable. Interestingly, the main differences between the general dynamic behaviors of the $A_{2A}AR$ and $A_{2B}AR$ explored can be explained in terms of their particular sequences, loops lengths, and disulfide bridges. The observed enhanced mobility of the extracellular part of the $A_{2B}AR$ could justify, to some extent, the lower affinity of this receptor for the natural ligand, adenosine,[83] as a function of the expected higher rate of diffusion of ligand molecules in the extracellular side. Accordingly, the consideration of a positively charged histidine in EL3 of the $hA_{2A}AR$ also reduces the mobility of the extracellular regions of this receptor. The conservation pattern shown in Figure S4 of the Supporting Information denotes that this histidine is only present in the A_1AR and $A_{2A}AR$, which are precisely the receptors in the family showing the highest affinity for adenosine. These observations reinforce the idea that the different composition of the extracellular region surrounding the binding site is modulating ligand affinity, recently proposed by us in the design of hA_3AR ligands,[84] as well as by other authors on the basis of sequence analysis and site-directed mutagenesis studies.[85] Interestingly, the crystal structure of the $A_{2A}AR$ in complex with an agonist, which has been released while this paper was being revised,[86] shows a disruption of the interactions between EL2 and EL3 to accommodate the bulky substitution at the N6 exocyclic amino group of the cocrystallized ligand. We thus find this experimental result in good agreement with the simulations reported herein, in which the lid formed by these loops tends to open in the absence of any ligand.

We also investigated the structural role of another relevant histidine located at position 7.43 in all ARs. The behavior of the interaction between the Glu1.39−His7.43 conserved pair is somehow surprising. Both in the apo form and in complex with the antagonist, this interaction fluctuates in the best cases or is even broken in some replicas. Conversely, when the charged form of this histidine is considered, the Glu1.39−His7.43 ionic pair is maintained along the whole MD simulation (see Figure 3C, simulation R1″). These results should be contextualized with the mutagenesis data available for this particular pair of residues. In the $A_{2A}AR$, a mutation of His7.43 to either Asp or Glu does not produce any detectable changes in either agonist or antagonist binding.[87] In this case, pK_a calculations predict that at least one of the two interacting residues should be modeled in its neutral, protonated form (see Figure S6 of the Supporting Information), which could thus be used to argue against the possibility of a salt bridge interaction between Glu1.39 and His7.43 on the wild-type receptor. However, a polar interaction between side chains at these positions may be a minimum condition for the integrity of the binding site, as a His7.43Ala mutant yields no detectable agonist or antagonist binding.[88] Finally, it should be noted that a Glu1.39Gln mutant has little effect on agonist binding, which is more affected by a His7.43Tyr mutation,[78] which led to the idea of position 7.43 interacting with the ribose moiety,[79] recently confirmed by the crystal structure of the agonist-bound $A_{2A}AR$.[86] Altogether, these data support a polar interaction between the aforementioned positions in TM1 and TM7, which is presented as a weak, intermittent interaction according to our MD simulations (Figure 3C, simulations R1, R2, R1′, and R2′), allowing a gradual separation of TM1 and TM7 that could be related to the conformational equilibrium of the receptor. Alternatively, the hypothesis of a salt bridge

occurring between these residues implies that no separation between these helices occurs along the simulation time, precluding a dynamic role of this pair of residues in the modulation of receptor conformations. The reliability of this alternate hypothesis should be tested with the expression and pharmacological characterization of a mutant receptor where His7.43 is replaced with a positively charged residue (Lys), as modeled in Figure S6 of the Supporting Information.

Several important dynamic properties, which prompt novel receptor interactions not observed in the crystal structure of the inactive A_{2A}AR, are reported and related to the conformational equilibrium of the ARs. First, the ionic lock, linking the (D/E)RY motif in TM3 with Glu6.30 in TM6, which is absent in the starting receptor structures, is spontaneously formed in the MD simulations presented. The fact that the ionic lock was also broken in the crystal structures of the β-adrenergic receptors has received much attention in the recent computational studies of this receptor family. The conclusions extracted from independent microsecond MD simulations[26,27] suggest that either the removal of T4 lysozyme or the absence of the G protein in the crystal structures might favor the formation of the ionic lock. The observation of this event in the initial steps of our MD simulations of the ARs, and the subsequent approach of the cytoplasmic part of the TM3 and TM6 helices, are in agreement with this hypothesis and with recently reported MD simulations of the A_{2A}AR,[36] while other authors have noted that such a conformational change is observed only at high saline concentrations in the same receptor.[30] Our results support the idea of a more complex network of hydrogen bonds and salt bridges stabilizing the ionic lock, where all four polar interactions considered among residues Thr2.39, Asp3.49, Tyr3.60, Arg3.50, and Glu6.30 are quite stable in our simulations (see Table 3). Interestingly, the importance of the salt bridge between the conserved Asp3.49 and Arg3.50 [within the (D/E)RY motif in TM3] has been identified with infrared spectroscopy experiments in rhodopsin[21] and was supported by previous experiments with the β2 receptor.[20]

A second event that we have identified is the spontaneous formation of the toggle switch in TM6, a closer look at which reveals novel structural elements in the ARs that deserve further analysis. In particular, the rotation of the side chain of Trp6.48 is accompanied in our simulations by a concerted rotameric transition of His6.52, a typical residue of the AR family with the only exception being the A_3AR. Interestingly, a histidine is also present at this position on the ghrelin receptor, where its key role in the basal activity of that receptor was postulated and experimentally verified.[89] Moreover, our simulations have revealed additional contacts of His6.52 with Phe5.43 and Asn5.42. Available mutagenesis data on the A_{2A}AR indicate that mutation of any of these three residues by an alanine precludes the detection of ligand binding,[88] which is partially reverted by the restoration of aromatic side chains in position 6.52 or 5.43 or a polar amino acid (Ser) at position 5.42. The phenylalanine at position 5.43 plays a role in the packing between TM5 and TM6, but we did not observe any conformational change for this residue in any of the independent MD simulations considered. This result is in contrast with the conclusions extracted from the recent MD simulations of the hA_{2A}AR by Lyman et al.,[36] who suggested that the occurrence of the toggle switch should be associated with conformational changes in residue Phe^{182} (5.43). In fact, such an association was motivated by the assignment of this residue to position 5.47 by the authors, and not to actual position 5.43, thus being incorrectly aligned with the Phe5.47 that is part of the highly conserved aromatic cluster of the aminergic receptor family.[90] Remarkably, residues at both positions 5.47 and 6.52 are conserved in the A_1AR, A_{2A}AR, and A_{2B}AR, with a small valine at position 5.47 favoring the rotameric transition of His6.52. Conversely, a correlated mutation is observed in all A_3ARs, where the histidine in position 6.52 is substituted with a Ser while a more bulky Ile substitutes for the otherwise subtype-conserved Val5.47. This evolutionary mechanism of a correlated mutation in positions 5.47 and 6.52 further reinforces the idea of a structural role of this pair of positions. The network of interactions that stabilize this microenvironment of the toggle switch in the A_2ARs reveals a previously unobserved dynamic role of polar residues Asn5.42 and Gln3.37. Our simulations indicate that the new connections established among transmembrane helices TM3, TM5, and TM6 are crucial for the receptor architecture or even the activation process, which might provide further explanation for the site-directed mutagenesis available for Gln3.37[91,92] and Asn5.42,[88] in contrast with the hypothesis formulated before the release of the A_{2A}AR crystallographic structure that had connected Gln3.37 with ligand binding.[87] This result is in agreement with the activation mechanism proposed in light of the new structures of agonist-bound β-adrenoreceptors, released during the preparation of this work.[17,18] In that family of GPCRs, the main variation in the experimental conformation of the agonist-bound receptor with respect to previous antagonist-bound structures is the new interaction between residues at positions 5.43 and 6.55 (one helix turn above His6.52), bringing TM5 and TM6 closer by ~1 Å[17] or even 2 Å.[18] However, the fully activated structures of the β2-adrenoreceptor[19] and opsin,[16] as well as the very recent crystal structure of the agonist-bound A_{2A}AR,[86] show no change in the side chain conformation of the highly conserved Trp6.48 (toggle switch). A recent hypothesis by the Schwartz group suggests that the switch of Trp6.48, which is only 70% conserved in the GPCR family, would be one of the many potential microswitches occurring during GPCR activation and thus would be dispensable in a given GPCR (i.e., β2-adrenoreceptor), which might still conserve a tryptophan in this position.[93] In other GPCRs, residue Trp6.48 would change the rotameric state in the initial steps of the activation process, as previously postulated by several authors,[22,90] preceding the higher-magnitude conformational changes observed in TM6.[16,19] In light of the new experimental evidence showing an unchanged rotameric state of Trp6.48 between the agonist- and antagonist-bound conformations of the A_{2A}AR, we hypothesize that the role of this switch is transient, promoting an intermediate conformation that would favor the achievement of major movements observed on TM6 in the active-like conformation of the A_{2A}AR. In fact, a closer look at the major conformational changes between the two crystal structures of this receptor reveals that the movement of the intracellular side of TM6 is accompanied by the rotameric transition of aromatic residues Phe5.62 and Tyr5.68, in the intracellular side of TM5.[86] To avoid steric clashes of these moving residues with TM6, this helix must visit a more open conformation different from that observed in either antagonist- or agonist-bound crystal structures, a conformation that might be promoted by the toggle switch and surrounding interaction network described in this work. Notably, the superposition of the end point conformation of the A_{2A}AR R1 simulation with the agonist-bound crystal structure shows a remarkable overlay of TM6 (see Figure S7 of the Supporting Information), which in both cases is shifted away from the TM bundle on its intracellular

side (that is, below the conserved proline kink). The observations reported herein suggest that further site-directed mutagenesis experiments with the aforementioned positions in helices TM5, TM6, and TM7, especially considering mutations less drastic than those previously reported, would shed light on the molecular mechanisms of AR activation.

■ ASSOCIATED CONTENT

Supporting Information. Supplementary Methods detailing trajectory analyses; structure of the A_{2A}AR replica with crystallographic waters (RW1), with a water occupancy analysis of the first hydration shell for the residues in the vicinity of the crystallographic waters (Figure S1); rmsd analysis of loop equilibration and production trajectories, and comparative rmsf analysis of RW1 (Figure S2); analysis of the conformational states of Asn7.45 (Figure S3); multiple-sequence alignment of EL3 of human ARs (Figure S4); PCA of the R1″ simulation (Figure S5); structural models and short MD simulations of mutant receptors for position 7.43 (Figure S6); and comparison of starting and end point structures belonging to the R1 simulation with the crystal structure of the agonist-bound A_{2A}AR (Figure S7). This material is available free of charge via the Internet at http://pubs.acs.org.

■ AUTHOR INFORMATION

Corresponding Author

*E-mail: hugo.teran@usc.es. Phone: +34 881813873. Fax: +34981951473.

Funding Sources

Funding from the Xunta de Galicia, Consellería de Sanidade (Grant PS09/63), and the Spanish Ministry of Science and Innovation (2010 ICTS Project) is gratefully acknowledged. Á.P. and H.G.-d.-T. are researchers of the Isidro Parga Pondal program (Xunta de Galicia, Spain). D.R. is a recipient of a predoctoral grant from the Fondo de Investigación Sanitaria (ISCIII, MICINN).

■ ACKNOWLEDGMENT

Computations were conducted at the resources of the Galician Supercomputing Center (CESGA). We thank Pilar Brocos for assistance in the design of automated protocols. We acknowledge reviewer 1 for important suggestions that contributed to improve this manuscript.

■ ABBREVIATIONS

AR, adenosine receptor; GPCR, G protein-coupled receptor; EL and IL, extracellular and intracellular loops, respectively; MD, molecular dynamics; POPC, palmitoyloleoylphosphatidylcholine; PCA, principal component analysis; rmsd, root-mean-square deviation; rmsf, root-mean-square fluctuation; TM, transmembrane; hA_{2A}AR and hA_{2B}AR, human receptors; A_{2A} and A_{2B}, adenosine receptors; D_3DR, D_3 dopamine receptor; tβ1, turkey β1-adrenergic receptor; hβ2, human β2-adrenergic receptor; *g+*, *gauche+*; *t*, *trans*.

■ REFERENCES

(1) Rosenbaum, D. M., Rasmussen, S. G., and Kobilka, B. K. (2009) The structure and function of G-protein-coupled receptors. *Nature 459*, 356–363.

(2) Kenakin, T. (2004) Principles: Receptor theory in pharmacology. *Trends Pharmacol. Sci. 25*, 186–192.

(3) Hanson, M. A., and Stevens, R. C. (2009) Discovery of new GPCR biology: One receptor structure at a time. *Structure 17*, 8–14.

(4) Fredriksson, R., Lagerström, M. C., Lundin, L.-G., and Schiöth, H. B. (2003) The G-protein-coupled receptors in the human genome form five main families. Phylogenetic analysis, paralogon groups, and fingerprints. *Mol. Pharmacol. 63*, 1256–1272.

(5) Jacobson, K. A., and Gao, Z.-G. (2006) Adenosine receptors as therapeutic targets. *Nat. Rev. Drug Discovery 5*, 247–264.

(6) Ohta, A., and Sitkovsky, M. (2001) Role of G-protein-coupled adenosine receptors in downregulation of inflammation and protection from tissue damage. *Nature 414*, 916–920.

(7) Kalla, R. V., and Zablocki, J. (2009) Progress in the discovery of selective, high affinity A(2B) adenosine receptor antagonists as clinical candidates. *Purinergic Signalling 5*, 21–29.

(8) Downey, J. M., Liu, G. S., and Thornton, J. D. (1993) Adenosine and the anti-infarct effects of preconditioning. *Cardiovasc. Res. 27*, 3–8.

(9) Miller, D. D. (2005) Impact of selective adenosine A2A receptor agonists on cardiac imaging feeling the lightning, waiting on the thunder. *J. Am. Coll. Cardiol. 46*, 2076–2078.

(10) Fredholm, B. B., Arslan, G., Kull, B., and Svenningsson, P. (1998) Locating the neuronal targets for caffeine. *Drug Dev. Res. 45*, 324–328.

(11) Franco, R., Ferre, S., Torvinen, M., Gines, S., Hillion, J., Ciruela, F., Canela, E. I., Mallol, J., Casado, V., Lluis, C., and Fuxe, K. (2001) Adenosine/dopamine receptor-receptor interactions in the central nervous system. *Drug Dev. Res. 52*, 296–302.

(12) Jaakola, V.-P., Griffith, M. T., Hanson, M. A., Cherezov, V., Chien, E. Y. T., Lane, J. R., Ijzerman, A. P., and Stevens, R. C. (2008) The 2.6 angstrom crystal structure of a human A2A adenosine receptor bound to an antagonist. *Science 322*, 1211–1217.

(13) Cherezov, V., Rosenbaum, D. M., Hanson, M. A., Rasmussen, S. G. F., Thian, F. S., Kobilka, T. S., Choi, H.-J., Kuhn, P., Weis, W. I., Kobilka, B. K., and Stevens, R. C. (2007) High-resolution crystal structure of an engineered human β2-adrenergic G protein-coupled receptor. *Science 318*, 1258–1265.

(14) Jaakola, V.-P., Prilusky, J., Sussman, J. L., and Goldman, A. (2005) G protein-coupled receptors show unusual patterns of intrinsic unfolding. *Protein Eng., Des. Sel. 18*, 103–110.

(15) Martinelli, A., and Tuccinardi, T. (2008) Molecular modeling of adenosine receptors: New results and trends. *Med. Res. Rev. 28*, 247–277.

(16) Park, J. H., Scheerer, P., Hofmann, K. P., Choe, H.-W., and Ernst, O. P. (2008) Crystal structure of the ligand-free G-protein-coupled receptor opsin. *Nature 454*, 183–187.

(17) Warne, T., Moukhametzianov, R., Baker, J. G., Nehme, R., Edwards, P. C., Leslie, A. G., Schertler, G. F., and Tate, C. G. (2011) The structural basis for agonist and partial agonist action on a β_1-adrenergic receptor. *Nature 469*, 241–244.

(18) Rosenbaum, D. M., Zhang, C., Lyons, J. A., Holl, R., Aragao, D., Arlow, D. H., Rasmussen, S. G., Choi, H. J., Devree, B. T., Sunahara, R. K., Chae, P. S., Gellman, S. H., Dror, R. O., Shaw, D. E., Weis, W. I., Caffrey, M., Gmeiner, P., and Kobilka, B. K. (2011) Structure and function of an irreversible agonist-β_2 adrenoceptor complex. *Nature 469*, 236–240.

(19) Rasmussen, S. G., Choi, H. J., Fung, J. J., Pardon, E., Casarosa, P., Chae, P. S., Devree, B. T., Rosenbaum, D. M., Thian, F. S., Kobilka, T. S., Schnapp, A., Konetzki, I., Sunahara, R. K., Gellman, S. H., Pautsch, A., Steyaert, J., Weis, W. I., and Kobilka, B. K. (2011) Structure of a nanobody-stabilized active state of the β_2 adrenoceptor. *Nature 469*, 175–180.

(20) Ballesteros, J. A., Jensen, A. D., Liapakis, G., Rasmussen, S. G., Shi, L., Gether, U., and Javitch, J. A. (2001) Activation of the β2-adrenergic receptor involves disruption of an ionic lock between the cytoplasmic ends of transmembrane segments 3 and 6. *J. Biol. Chem. 276*, 29171–29177.

(21) Vogel, R., Mahalingam, M., Lüdeke, S., Huber, T., Siebert, F., and Sakmar, T. P. (2008) Functional role of the "ionic lock": An

interhelical hydrogen-bond network in family A heptahelical receptors. *J. Mol. Biol. 380*, 648–655.

(22) Shi, L., Liapakis, G., Xu, R., Guarnieri, F., Ballesteros, J. A., and Javitch, J. A. (2002) β2 adrenergic receptor activation. Modulation of the proline kink in transmembrane 6 by a rotamer toggle switch. *J. Biol. Chem. 277*, 40989–40996.

(23) Audet, M., and Bouvier, M. (2008) Insights into signaling from the β2-adrenergic receptor structure. *Nat. Chem. Biol. 4*, 397–403.

(24) Kobilka, B. K., and Deupi, X. (2007) Conformational complexity of G-protein-coupled receptors. *Trends Pharmacol. Sci. 28*, 397–406.

(25) Chien, E. Y. T., Liu, W., Zhao, Q., Katritch, V., Han, G. W., Hanson, M. A., Shi, L., Newman, A. H., Javitch, J. A., Cherezov, V., and Stevens, R. C. (2010) Structure of the human dopamine D3 receptor in complex with a D2/D3 selective antagonist. *Science 330*, 1091–1095.

(26) Vanni, S., Neri, M., Tavernelli, I., and Rothlisberger, U. (2009) Observation of "ionic lock" formation in molecular dynamics simulations of wild-type β_1 and β_2 adrenergic receptors. *Biochemistry 48*, 4789–4797.

(27) Dror, R. O., Arlow, D. H., Borhani, D. W., Jensen, M. Ø., Piana, S., and Shaw, D. E. (2009) Identification of two distinct inactive conformations of the β2-adrenergic receptor reconciles structural and biochemical observations. *Proc. Natl. Acad. Sci. U.S.A. 106*, 4689–4694.

(28) Romo, T. D., Grossfield, A., and Pitman, M. C. (2010) Concerted interconversion between ionic lock substates of the β_2 adrenergic receptor revealed by microsecond timescale molecular dynamics. *Biophys. J. 98*, 76–84.

(29) Huber, T., Menon, S., and Sakmar, T. P. (2008) Structural basis for ligand binding and specificity in adrenergic receptors: Implications for GPCR-targeted drug discovery. *Biochemistry 47*, 11013–11023.

(30) Jójárt, B. z., Kiss, R. b., Viskolcz, B. l., Kolossváry, I. n., and Keserü, G. r. M. (2010) Molecular Dynamics Simulation at High Sodium Chloride Concentration: Toward the Inactive Conformation of the Human Adenosine A2A Receptor. *J. Phys. Chem. Lett. 1*, 1008–1013.

(31) Hu, J., Wang, Y., Zhang, X., Lloyd, J. R., Li, J. H., Karpiak, J., Costanzi, S., and Wess, J. (2010) Structural basis of G protein-coupled receptor-G protein interactions. *Nat. Chem. Biol. 6*, 541–548.

(32) Kolb, P., Rosenbaum, D. M., Irwin, J. J., Fung, J. J., Kobilka, B. K., and Shoichet, B. K. (2009) Structure-based discovery of β2-adrenergic receptor ligands. *Proc. Natl. Acad. Sci. U.S.A. 106*, 6843–6848.

(33) Bhattacharya, S., Hall, S. E., and Vaidehi, N. (2008) Agonist-induced conformational changes in bovine rhodopsin: Insight into activation of G-protein-coupled receptors. *J. Mol. Biol. 382*, 539–555.

(34) Provasi, D., and Filizola, M. (2010) Putative active states of a prototypic g-protein-coupled receptor from biased molecular dynamics. *Biophys. J. 98*, 2347–2355.

(35) Carlsson, J., Yoo, L., Gao, Z.-G., Irwin, J. J., Shoichet, B. K., and Jacobson, K. A. (2010) Structure-based discovery of A2A adenosine receptor ligands. *J. Med. Chem. 53*, 3748–3755.

(36) Lyman, E., Higgs, C., Kim, B., Lupyan, D., Shelley, J. C., Farid, R., and Voth, G. A. (2009) A role for a specific cholesterol interaction in stabilizing the Apo configuration of the human A_{2A} adenosine receptor. *Structure 17*, 1660–1668.

(37) Baldwin, J. M., Schertler, G. F., and Unger, V. M. (1997) An α-carbon template for the transmembrane helices in the rhodopsin family of G-protein-coupled receptors. *J. Mol. Biol. 272*, 144–164.

(38) Mirzadegan, T., Benko, G., Filipek, S., and Palczewski, K. (2003) Sequence analyses of G-protein-coupled receptors: Similarities to rhodopsin. *Biochemistry 42*, 2759–2767.

(39) Mobarec, J. C., Sanchez, R., and Filizola, M. (2009) Modern homology modeling of G-protein coupled receptors: Which structural template to use? *J. Med. Chem. 52*, 5207–5216.

(40) Ballesteros, J. A., and Weinstein, H. (1995) Integrated methods for the construction of three dimensional models and computational probing of structure-function relations in G-protein coupled receptors. In *Methods in Neuroscience*, pp 366−428, Academic Press, San Diego.

(41) Sali, A., and Blundell, T. L. (1993) Comparative protein modelling by satisfaction of spatial restraints. *J. Mol. Biol. 234*, 779–815.

(42) Fiser, A., Do, R. K., and Sali, A. (2000) Modeling of loops in protein structures. *Protein Sci. 9*, 1753–1773.

(43) Laskowski, R. A., MacArthur, M. W., Moss, D. S., and Thornton, J. M. (1993) PROCHECK: A program to check the stereochemical quality of protein structures. *J. Appl. Crystallogr. 26*, 283–291.

(44) Davis, I. W., Leaver-Fay, A., Chen, V. B., Block, J. N., Kapral, G. J., Wang, X., Murray, L. W., Arendall, W. B., Snoeyink, J., Richardson, J. S., and Richardson, D. C. (2007) MolProbity: All-atom contacts and structure validation for proteins and nucleic acids. *Nucleic Acids Res. 35*, W375–W383.

(45) Dolinsky, T. J., Nielsen, J. E., McCammon, J. A., and Baker, N. A. (2004) PDB2PQR: An automated pipeline for the setup of Poisson-Boltzmann electrostatics calculations. *Nucleic Acids Res. 32*, W665–W667.

(46) Song, Y., Mao, J., and Gunner, M. R. (2009) MCCE2: Improving protein pKa calculations with extensive side chain rotamer sampling. *J. Comput. Chem. 30*, 2231–2247.

(47) Rocchia, W., Sridharan, S., Nicholls, A., Alexov, E., Chiabrera, A., and Honig, B. (2002) Rapid grid-based construction of the molecular surface and the use of induced surface charge to calculate reaction field energies: Applications to the molecular systems and geometric objects. *J. Comput. Chem. 23*, 128–137.

(48) Song, Y., Mao, J., and Gunner, M. R. (2003) Calculation of proton transfers in bacteriorhodopsin bR and M intermediates. *Biochemistry 42*, 9875–9888.

(49) *Macromodel* (2009) Schrödinger, LLC, New York.

(50) Jorgensen, W. L., Maxwell, D. S., and Tirado-Rives, J. (1996) Development and testing of the OPLS all-atom force field on conformational energetics and properties of organic liquids. *J. Am. Chem. Soc. 118*, 11225–11236.

(51) Kaminski, G. A., Friesner, R. A., Tirado-Rives, J., and Jorgensen, W. L. (2001) Evaluation and reparametrization of the OPLS-AA force field for proteins via comparison with accurate quantum chemical calculations on peptides. *J. Phys. Chem. B 105*, 6474–6487.

(52) Thompson, J. D., Gibson, T. J., Plewniak, F., Jeanmougin, F., and Higgins, D. G. (1997) The CLUSTAL:X windows interface: Flexible strategies for multiple sequence alignment aided by quality analysis tools. *Nucleic Acids Res. 25*, 4876–4882.

(53) Michino, M., Abola, E., Brooks, C. L., Dixon, J. S., Moult, J., and Stevens, R. C. (2009) Community-wide assessment of GPCR structure modelling and ligand docking: GPCR Dock 2008. *Nat. Rev. Drug Discovery 8*, 455–463.

(54) Chakrabarti, N., Neale, C., Payandeh, J., Pai, E. F., and Pomès, R. (2010) An iris-like mechanism of pore dilation in the CorA magnesium transport system. *Biophys. J. 98*, 784–792.

(55) Lindahl, E., and Edholm, O. (2000) Mesoscopic undulations and thickness fluctuations in lipid bilayers from molecular dynamics simulations. *Biophys. J. 79*, 426–433.

(56) Berger, O., Edholm, O., and Jähnig, F. (1997) Molecular dynamics simulations of a fluid bilayer of dipalmitoylphosphatidylcholine at full hydration, constant pressure, and constant temperature. *Biophys. J. 72*, 2002–2013.

(57) Berendsen, H. J. C., Postma, J. P. M., van Gunsteren, W. F., and Hermans, J. (1981) Interaction models for Water in Relation to Protein Hydration. In *Intermolecular Forces* (Pullman, B., Ed.) pp 331−342, D. Reidel Publishing Co., Dordrecht, The Netherlands.

(58) Nose, S., and Klein, M. L. (1983) Constant pressure molecular-dynamics for molecular systems. *Mol. Phys. 50*, 1055–1076.

(59) Parrinello, M., and Rahman, A. (1981) Polymorphic transitions in single-crystals: A new molecular-dynamics method. *J. Appl. Phys. 52*, 7182–7190.

(60) Essmann, U., Perera, L., Berkowitz, M. L., Darden, T., Lee, H., and Pedersen, L. G. (1995) A smooth particle mesh Ewald method. *J. Chem. Phys. 103*, 8577–8577.

(61) Darden, T., York, D., and Pedersen, L. (1993) Particle mesh Ewald: An N·log(N) method for Ewald sums in large systems. *J. Chem. Phys. 98*, 10089–10089.

(62) Hockney, R. W., and Eastwood, J. W. (1988) *Computer simulation using particles*, 1st ed., Adam Hilger, Bristol, U.K.

(63) Miyamoto, S., and Kollman, P. A. (1992) Settle: An analytical version of the SHAKE and RATTLE algorithm for rigid water models. *J. Comput. Chem. 13*, 952–962.

(64) Hess, B., Bekker, H., Berendsen, H. J. C., and Fraaije, J. G. E. M. (1997) LINCS: A linear constraint solver for molecular simulations. *J. Comput. Chem. 18*, 1463–1472.

(65) Hess, B., Kutzner, C., van der Spoel, D., and Lindahl, E. (2008) GROMACS 4: Algorithms for Highly Efficient, Load-Balanced, and Scalable Molecular Simulation. *J. Chem. Theory Comput. 4*, 435–447.

(66) Berendsen, H. J. C., van der Spoel, D., and Vandrunen, R. (1995) GROMACS: A message-passing parallel molecular-dynamics implementation. *Comput. Phys. Commun. 91*, 43–56.

(67) Klinger, M., Kuhn, M., Just, H., Stefan, E., Palmer, T., Freissmuth, M., and Nanoff, C. (2002) Removal of the carboxy terminus of the A2A-adenosine receptor blunts constitutive activity: Differential effect on cAMP accumulation and MAP kinase stimulation. *Naunyn-Schmiedeberg's Arch. Pharmacol. 366*, 287–298.

(68) Safhi, M. M., Rutherford, C., Ledent, C., Sands, W. A., and Palmer, T. M. (2010) Priming of signal transducer and activator of transcription proteins for cytokine-triggered polyubiquitylation and degradation by the A 2A adenosine receptor. *Mol. Pharmacol. 77*, 968–978.

(69) Angel, T. E., Chance, M. R., and Palczewski, K. (2009) Conserved waters mediate structural and functional activation of family A (rhodopsin-like) G protein-coupled receptors. *Proc. Natl. Acad. Sci. U. S.A. 106*, 8555–8560.

(70) Pardo, L., Deupi, X., Dölker, N., López-Rodríguez, M. L., and Campillo, M. (2007) The role of internal water molecules in the structure and function of the rhodopsin family of G protein-coupled receptors. *ChemBioChem 8*, 19–24.

(71) Angel, T. E., Gupta, S., Jastrzebska, B., Palczewski, K., and Chance, M. R. (2009) Structural waters define a functional channel mediating activation of the GPCR, rhodopsin. *Proc. Natl. Acad. Sci. U.S. A. 106*, 14367–14372.

(72) Freites, J. A., Tobias, D. J., von Heijne, G., and White, S. H. (2005) Interface connections of a transmembrane voltage sensor. *Proc. Natl. Acad. Sci. U.S.A. 102*, 15059–15064.

(73) Zhou, W., Flanagan, C., Ballesteros, J., Konvicka, K., Davidson, J., Weinstein, H., Millar, R., and Sealfon, S. (1994) A reciprocal mutation supports helix 2 and helix 7 proximity in the gonadotropin-releasing hormone receptor. *Mol. Pharmacol. 45*, 165–170.

(74) Liapakis, G., Chan, W. C., Papadokostaki, M., and Javitch, J. A. (2004) Synergistic contributions of the functional groups of epinephrine to its affinity and efficacy at the β2 adrenergic receptor. *Mol. Pharmacol. 65*, 1181–1190.

(75) Vanni, S., Neri, M., Tavernelli, I., and Rothlisberger, U. (2010) A conserved protonation-induced switch can trigger "ionic-lock" formation in adrenergic receptors. *J. Mol. Biol. 397*, 1339–1349.

(76) Selent, J., Sanz, F., Pastor, M., and De Fabritiis, G. (2010) Induced effects of sodium ions on dopaminergic G-protein coupled receptors. *PLoS Comput. Biol. 6*, e1000884.

(77) Lenzi, O., Colotta, V., Catarzi, D., Varano, F., Poli, D., Filacchioni, G., Varani, K., Vincenzi, F., Borea, P. A., Paoletta, S., Morizzo, E., and Moro, S. (2009) 2-Phenylpyrazolo[4,3-d]pyrimidin-7-one as a new scaffold to obtain potent and selective human A3 adenosine receptor antagonists: New insights into the receptor-antagonist recognition. *J. Med. Chem. 52*, 7640–7652.

(78) Gao, Z. G., Jiang, Q., Jacobson, K. A., and Ijzerman, A. P. (2000) Site-directed mutagenesis studies of human A_{2A} adenosine receptors: Involvement of Glu(13) and His(278) in ligand binding and sodium modulation. *Biochem. Pharmacol. 60*, 661–668.

(79) Ijzerman, A., van der Wenden, E. M., van Galen, P. J. M., and Jacobson, K. A. (1994) Molecular modelling of adenosine receptors. The ligand binding site on the rat adenosine A2A receptor. *Eur. J. Pharmacol. 268*, 95–104.

(80) Ijzerman, A. P., Kunzel, J. K. V. F. D., Kim, J., Qiaoling, J., and Jacobson, K. A. (1996) Site-directed mutagenesis of the human adenosine A2A receptor. Critical involvement of Glu13 in agonist recognition. *Eur. J. Pharmacol. 310*, 269–272.

(81) Morozov, A. V., Kortemme, T., Tsemekhman, K., and Baker, D. (2004) Close agreement between the orientation dependence of hydrogen bonds observed in protein structures and quantum mechanical calculations. *Proc. Natl. Acad. Sci. U.S.A. 101*, 6946–6951.

(82) Jiang, Q., Lee, B. X., Glashofer, M., van Rhee, A. M., and Jacobson, K. A. (1997) Mutagenesis reveals structure-activity parallels between human A2A adenosine receptors and biogenic amine G protein-coupled receptors. *J. Med. Chem. 40*, 2588–2595.

(83) Fredholm, B. B., Ijzerman, A. P., Jacobson, K. A., Klotz, K. N., and Linden, J. (2001) International Union of Pharmacology. XXV. Nomenclature and classification of adenosine receptors. *Pharmacol. Rev. 53*, 527–552.

(84) Yaziji, V., Rodriguez, D., Gutierrez-de-Teran, H., Coelho, A., Caamano, O., Garcia-Mera, X., Brea, J., Loza, M. I., Cadavid, M. I., and Sotelo, E. (2011) Pyrimidine derivatives as potent and selective A3 adenosine receptor antagonists. *J. Med. Chem. 54*, 457–471.

(85) Jaakola, V. P., Lane, J. R., Lin, J. Y., Katritch, V., Ijzerman, A. P., and Stevens, R. C. (2010) Ligand binding and subtype selectivity of the human A_{2A} adenosine receptor: Identification and characterization of essential amino acid residues. *J. Biol. Chem. 285*, 13032–13044.

(86) Xu, F., Wu, H., Katritch, V., Han, G. W., Jacobson, K. A., Gao, Z. G., Cherezov, V., and Stevens, R. C. (2011) Structure of an Agonist-Bound Human A2A Adenosine Receptor. *Science*.

(87) Kim, S. K., Gao, Z. G., Rompaey, P. V., Gross, A. S., Chen, A., Calenbergh, S. V., and Jacobson, K. A. (2003) Modeling the Adenosine Receptors: Comparison of the Binding Domains of A2A Agonists and Antagonists. *J. Med. Chem. 46*, 4847–4859.

(88) Kim, J., Wess, J., van Rhee, A. M., Schöneberg, T., and Jacobson, K. A. (1995) Site-directed Mutagenesis Identifies Residues Involved in Ligand Recognition in the Human A2A Adenosine Receptor. *J. Biol. Chem. 270*, 13987–13997.

(89) Floquet, N., M'Kadmi, C., Perahia, D., Gagne, D., Berge, G., Marie, J., Baneres, J. L., Galleyrand, J. C., Fehrentz, J. A., and Martinez, J. (2010) Activation of the ghrelin receptor is described by a privileged collective motion: A model for constitutive and agonist-induced activation of a sub-class A G-protein coupled receptor (GPCR). *J. Mol. Biol. 395*, 769–784.

(90) Schwartz, T. W., Frimurer, T. M., Holst, B., Rosenkilde, M. M., and Elling, C. E. (2006) Molecular mechanism of 7TM receptor activation: A global toggle switch model. *Annu. Rev. Pharmacol. Toxicol. 46*, 481–519.

(91) Rivkees, S. A., Barbhaiya, H., and Ijzerman, A. P. (1999) Identification of the Adenine Binding Site of the Human A1 Adenosine Receptor. *J. Biol. Chem. 274*, 3617–3621.

(92) Jiang, Q., Van Rhee, A., Kim, J., Yehle, S., Wess, J., and Jacobson, K. (1996) Hydrophilic side chains in the third and seventh transmembrane helical domains of human A2A adenosine receptors are required for ligand recognition. *Mol. Pharmacol. 50*, 512–521.

(93) Nygaard, R., Frimurer, T. M., Holst, B., Rosenkilde, M. M., and Schwartz, T. W. (2009) Ligand binding and micro-switches in 7TM receptor structures. *Trends Pharmacol. Sci. 30*, 249–259.